Journal of Alloys and Compounds 643 (2015) S99–S106

Contents lists available at ScienceDirect

Journal of Alloys and Compounds

journal homepage: www.elsevier.com/locate/jalcom

Nanoquasicrystalline Al-based matrix/γ-Al_2O_3 nanocomposites

M. Galano [a,*], A. Marsh [a], F. Audebert [a,b,c], W. Xu [a], M. Ramundo [a,d]

[a] Department of Materials, University of Oxford, Parks Road, OX1 3PH Oxford, UK
[b] Advanced Materials Group, INTECIN, Faculty of Engineering, University of Buenos Aires, Paseo Colón 850, Ciudad de Buenos Aires 1063, Argentina
[c] Department of Mechanical Engineering and Mathematical Sciences, Oxford Brookes University, Wheatley Campus, OX33 1HX Oxford, UK
[d] Department of Materials Science and Engineering, Massachusetts Institute of Technology, United States

ARTICLE INFO

Article history:
Available online 23 December 2014

Keywords:
Metal matrix composites
Quasicrystals
Aluminium
Ball milling

ABSTRACT

Quasicrystalline aluminium alloys have been studied in the past years achieving higher strength than commercial Al alloys and retaining high strength at high temperature. In this work a quasicrystalline Al alloy matrix nanocomposite containing nanoceramic particles has been manufactured using ball milling and hot extrusion. For that purpose a nanoquasicrystalline Al–Fe–Cr–Ti alloy was manufactured by powder atomisation. Nanocomposites consisting of a quasicrystalline Al–Fe–Cr–Ti alloy matrix and reinforcement of γ-Al_2O_3 nano particles were manufactured. The effect of ball milling time on the microstructure and microhardness of the nanocomposite powders was investigated. Bulk materials were produced by consolidation and hot extrusion. The microstructure and microhardness of the extruded materials were characterised.

The milling regime behaviour is discussed, and shows three different steps that have a significant effect on the rate of change of uniformity of the reinforcement distribution, matrix microstructure, powder size distribution and its microhardness. No significant decomposition of the quasicrystalline phase occurred over 30 h of milling. Strain increased and the crystallite size of the aluminium phase decreased with milling time, with the Al crystallite size reaching a steady state. Although the quasicrystalline phase decomposed during hot extrusion, the microhardness of the nanocomposite produced is significantly harder (227 ± 3 μHV_{500}) than both the unreinforced quasicrystalline alloy (159 ± 1 μHV_{500}) and crystalline aluminium nanocomposites reported in the literature [1]. Methods and analysis of material behaviour put forward in this work inform further understanding and optimisation of this and other nanocomposite systems containing a metastable microstructure matrix.

1. Introduction

Compared with commercial Al alloys, the nanoquasicrystalline Al–Fe–Cr based alloys, have proven to have outstanding mechanical properties which give them a considerable prospect for industry applications, such as in automotive and aeronautic applications due to their high strength at elevated temperatures and yet light weight [2,3]. Audebert et al. investigated and compared different series of nanostructured (nanocrystalline, nanoquasicrystalline, and nanogranular amorphous) Al based alloys, and found that the $Al_{93}Fe_3Cr_2Ti_2$ (at.%) alloy has a good combination of properties such as high strength, good thermal stability and good ductility [4]. The microstructure of the $Al_{93}Fe_3Cr_2Ti_2$ alloy in particular, consists of spherical icosahedral quasicrystalline particles (IQC) embedded in a crystalline α-Al matrix. Nanoquasicrystalline Al–Fe–Cr–Ti-based alloys with icosahedral quasicrystalline particles with around 100 nm embedded in an α-Al matrix can be produced by melt spinning [5]. In addition, gas atomization is another processing route that has been used to manufacture these nanoquasicrystalline Al–Fe–Cr–Ti alloys and the powder atomisation production was investigated in a previous work by Rounthwaite [6]. The powders microstructure were characterised and mechanical properties of hot extruded bars were measured at room temperature and elevated temperatures [6,7]. It was observed that the icosahedral quasicrystalline phase can be retained after the atomization in powder sizes typically under 75 μm, and also after the extrusion at 375 °C. The IQC particles in the 25–50 μm size fraction of gas atomised $Al_{93}Fe_3Cr_2Ti_2$ alloy were observed with different sizes generally under 500 nm and having an estimated volume fraction of ~0.45 in the alloy [7,4].

Todd et al. reported that the bulk $Al_{93}Fe_3Cr_2Ti_2$ alloy has a significantly high strength of 545 MPa at room temperature and of 360 MPa at 250 °C with a Young Modulus of 82 GPa at room

* Corresponding author.
E-mail address: marina.galano@materials.ox.ac.uk (M. Galano).

http://dx.doi.org/10.1016/j.jallcom.2014.12.063
0925-8388/

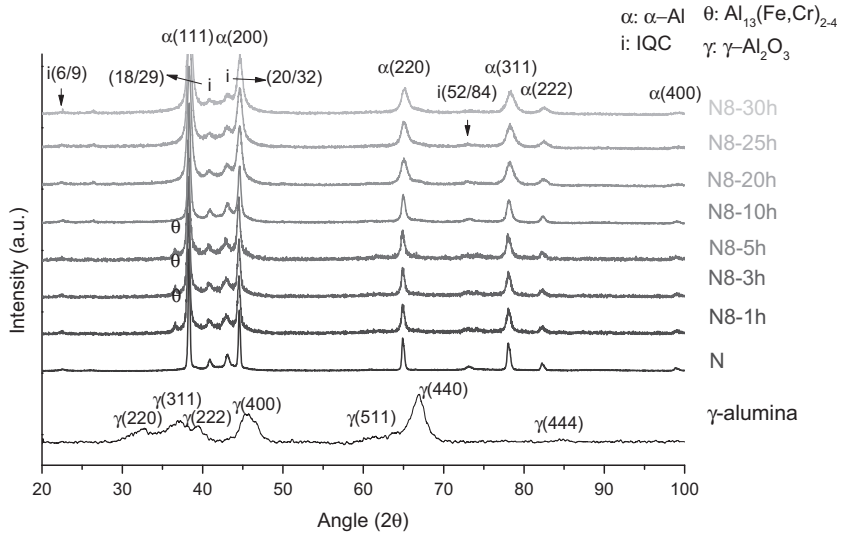

Fig. 1. X-ray diffractograms of the as-atomised N powder, Al_2O_3 powder and ball milled N8 powder samples from 1 to 30 h milling time.

temperature and ~60 GPa at 250 °C [7]. Therefore, it is particularly relevant to see the ways of increasing the strength and the Young's Modulus of this nanoquasicrystalline alloy to obtain a very competitive material with Ti alloys at an intermediate temperature range. Thus, a composites approach is needed.

Aluminium based nanocomposites (with reinforcements' sizes less than 500 nm) are another kind of relevant material for aircraft and automotive industries because of their high strength to weight ratio, high stiffness and wear-resistance. Mixing nanoparticles (<500 nm) increases the toughness and strength as particle and matrix bonding tends to improve as particle size get smaller, so interface decohesion tends not to occur [8]. For example, Tavoosi et al. fabricated the Al-13.8 wt.%Zn/5 vol.%Al_2O_3 nanocomposite, which has a microhardness of 185 HV, much higher than the Al-13.8 wt.%Zn alloy (150 HV) [9]. Some other studies are found in literature on ball milling Al6063 with nanosize Al_2O_3 (1.5 wt.%) obtaining a good uniformity of distribution and an increase in UTS from 241 MPa to 457 MPa and yield strength for 175–429 MPa [10].

To the best of the authors' knowledge, in the literature there are no previous reports on ball milling manufacturing of aluminium nanocomposites with nanoquasicrystalline Al based alloys as the matrix and nanoceramic particles as reinforcement. One of the main challenges of processing such material is achieving a homogeneous distribution of nano-sized alumina. It is supposed that high energy ball milling, which welds, breaks the powders and re-welds the powder particles, is a powerful way to solve this issue [9–12,13]. Considering that the quasicrystalline phase in Al–Fe–Cr–Ti alloys is metastable [5], another main challenge is to maintain the quasicrystal during the milling and extrusion processes.

In the present work, ball milling was used to manufacture nanoquasicrystalline Al alloy matrix nanocomposites with good homogeneous distribution of alumina and mechanical properties. Hot extrusion was used to make material in bulk shape. The improved mechanical behaviour and yet light weight of these nanocomposites could make them appealing for the automotive and aeronautic industries.

2. Experimental procedure

Nanoquasicrystalline gas-atomised powder with a composition of $Al_{93}Fe_3Cr_2Ti_2$ (N alloy) was produced in collaboration with Alpoco Ltd. and sieved in the 25–50 μm range. A Fritsch Mono Mill Pulverisette 6 Classic was used, with a 250 ml volume stainless steel milling vessel and milling balls of 10 mm diameter to prepare samples of the N alloy powder with reinforcement volume fractions of 8.5vol.% γ-alumina powder of 99.99% purity and average particle size 20–50 nm. The milling was carried out under positive argon pressure at a 250 rpm speed, initial balls to powder ratio of 10:1 and milling intervals of 1 h with pauses of 20 min after each hour. To assess the effect of varying milling time small quantity of powder was taken out of the milling vessel every hour up to 5 h then as a second batch, every 5 h from 10 up to 30 h of milling maintaining a ball to powder ratio between 10:1 and 12:1. Powders with different milling times were subsequently characterised. The milled powder is referred to as N8-*x* (where *x* is milling time in hours).

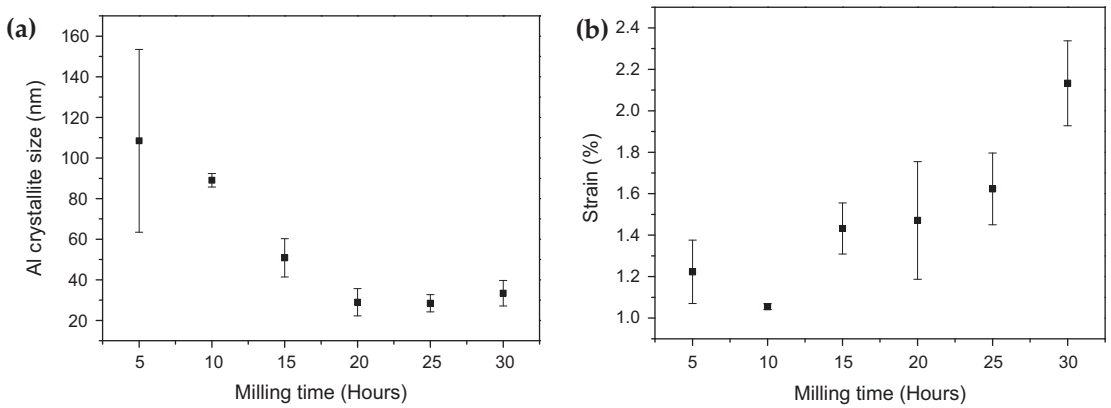

Fig. 2. (a) α-Al crystallite average size against milling time for the range of 5–30 h. (b) Strain in the α-Al phase against milling time for the range of 5–30 h.

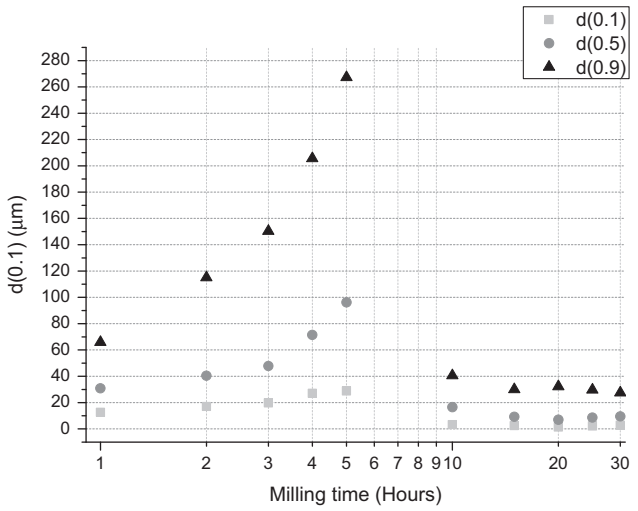

Fig. 3. Size distribution plot of the diameter of the 10th percentile, $d(0.1)$, the median, $d(0.5)$, and the 90th percentile, $d(0.9)$, of the N8 powder samples plotted against the logarithm of milling time.

Several batches of ball milled powders of 3 h milling time (N8-3) were cold compacted using a uniaxial cold press at 50 tonnes load. Compacted billets of N8 and pure N powder were extruded with an extrusion ratio of 16 and with an estimated extrusion temperature of 475 ± 20 °C, extrusion speed of 12.5 mm s^{-1} and 650 kN load.

A Malvern Mastersizer 2000 was used to measure powder particle size distribution. Samples of approximately 150 mg were deagglomerated with 1 min of ultrasonic vibration before analysis, to obtain a more accurate size distribution measurement.

X-ray diffractograms (XRD) were obtained with a Philips-1810 θ–2θ diffractometer with 0.15418 nm wavelength Cu Kα radiation at 35 kV and 50 mA, with scan conditions of 2θ range of 10–100° step size of 0.02° and scan rate of 0.01°/s.

Powders and extruded samples microstructure were analysed by a Jeol 2000FX and a Jeol 2100 transmission electron microscopes (TEM) with energy dispersive of X-ray (EDX) detector to obtain the approximated chemical compositions of the different phases. A FEI 200 focus ion beam (FIB) was used to observe the reinforcement distribution by milling away the surface oxide layer and for preparing lift-out TEM samples with average thickness of 130 nm.

A Thermal Advantage 2010 differential scanning calorimeter (DSC) was used at a heating rate of 40 K/min until 600 °C with Cu pans. The sample was placed between molybdenum discs. A 10 grams-force (gf) load was used for microindentations on the powders and a 500 gf load was used for the bulk samples with 15 s of dwell time. Microhardness was measured 20 times for each sample.

3. Results and discussions

3.1. Powder characterisation

3.1.1. Microstructural characterisation

The X-ray diffractogram for the N powder is given in Fig. 1. The metastable IQC phase has been formed with the α-Al. No intermetallics were observed. Peak positions at 2θ angles of 22.5, 40.9, 43.1, 61.0, 73.1 were identified for the IQC phase labelled using the Cahn's notation [14]. The XRD for the γ-alumina powder is also

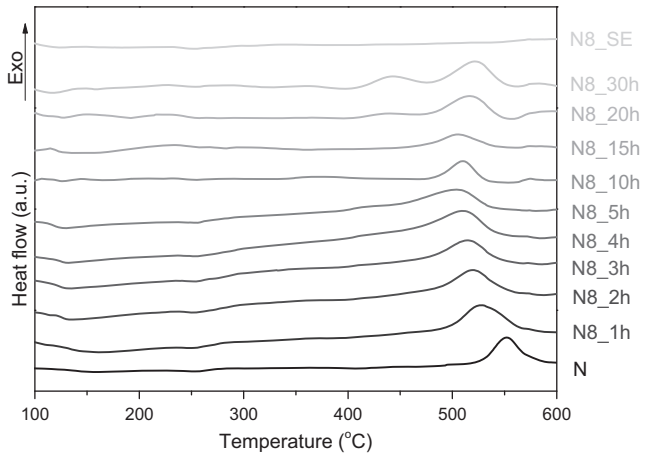

Fig. 5. DSC curves at 40 K/min for the N powder, the N8 powders milled from 1 to 30 h, and the N8-SE extruded composite.

given at the bottom in Fig. 1, γ-Al_2O_3 peaks are broad and the main peaks of the cubic γ-Al_2O_3 phase can be overlapped with the main peaks of the other phases of alumina, such as the monoclinic phase. The relative intensities between peaks differ from the reference pattern [15], especially between the (400) and (440) planes with peaks at 45.6°(2θ) and 66.9°(2θ) respectively. In a study into commercial γ-Al_2O_3 nanopowders [16], the authors attributed this phenomenon to "differences in site occupancies within the unit cell", suggesting possible causes to be anisotropic crystal shape or the presence of another Al_2O_3 phase, since γ-Al_2O_3 is the most thermodynamically stable Al_2O_3 phase at room temperature and for nanosize particles <13 nm in size [16].

XRD for the N8 composite for milling times of 0–30 h are also shown in Fig. 1. The IQC phase was identified together with the α-Al. Only a peak at $2\theta = 36.6$ indexed as corresponding to the metastable θ-$Al_{13}(Fe,Cr)_{2-4}$ phase was observed for powders milled for 1 h up to 5 h. The distorted θ-$Al_{13}(Cr,Fe)_{2-4}$ phase is a metastable phase with an undetermined composition and lattice parameter between those of the stable monoclinic phases $Al_{13}Fe_4$ and $Al_{13}Cr_2$ that have been observed in rapid solidified samples [4,5,17]. Broadening of all the peaks was observed, becoming more prominent as milling time progressed. The deformation involved in ball milling suggests that this broadening is due to distortion of the crystal and quasicrystal lattices through strain and the decreased crystallite size. The change of shape of the (18/29) and (20/32) IQC peaks suggests there could be some IQC decomposition; however, this is not possible to prove because of the overlapping between these IQC peaks and the main peaks of the stable $Al_{13}Fe_4$ and $Al_{13}Cr_2$ phases.

The highest intensity Al_2O_3 peaks, corresponding to the (400) and (440) planes, are not discernible in the XRD of the milled powders. This is likely due to a combination of the low volume fraction

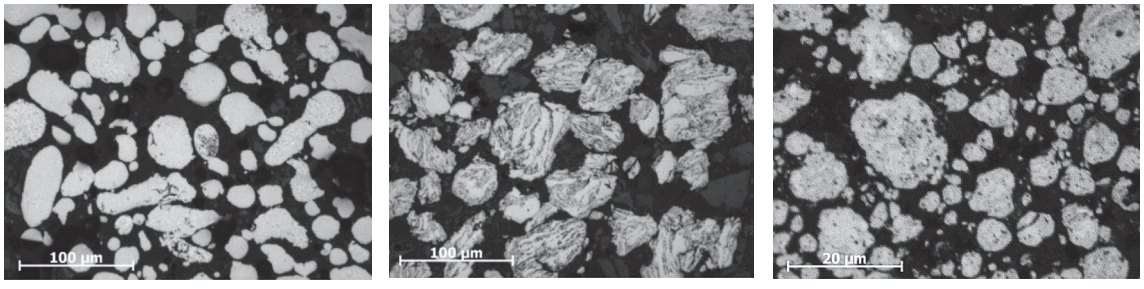

Fig. 4. Optical micrographs of the (a) nanoquasicrystalline Al alloy powders without alumina (N), (b) after 5 h of milling (N8-5), and (c) after 30 h of milling (N8-30).

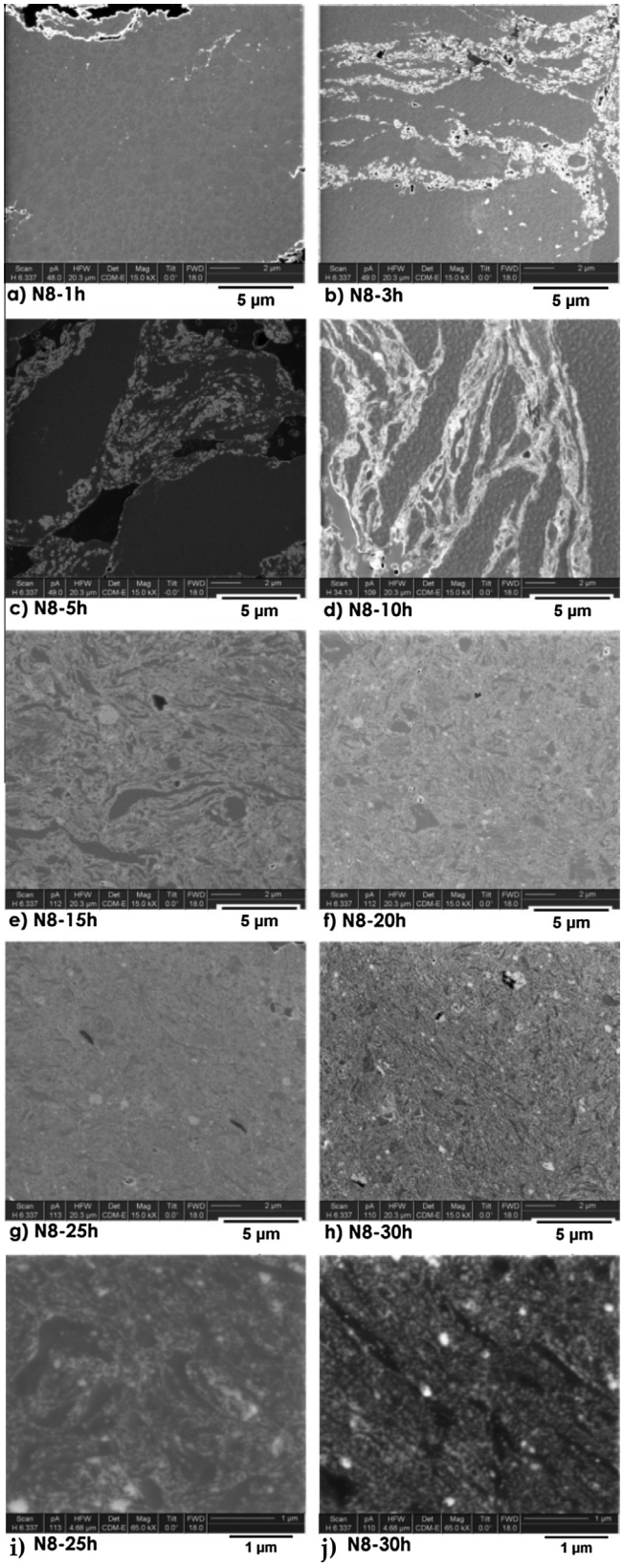

Fig. 6. FIB images of the N8 sample (a–h) at milling times of 1–30 h, (i and j) higher magnification of N8 sample milled for 25 and 30 h respectively.

of the Al_2O_3 in N8, and the broad and low intensity of the Al_2O_3 peaks as seen in Fig. 1.

Williamson–Hall analysis obtains a semi-quantitative measurements of crystallite size and strain by examining the broadening of the phase's XRD peaks relative to a reference specimen [18]. The full-width half maximum (FWHM) values for peaks of a specific phase are measured in the sample of interest, as well as in a reference sample which has no internal strain and a crystallite size of >500 nm. (1), Warren formula [18], is used to estimate the contribution of size and strain effects to the FWHM of each peak; where B = broadening in FWHM of a sample's peak due to size and strain effects, B_M = FWHM of a peak in a sample, B_S = FWHM of a peak in a reference sample (instrumental broadening).

$$B^2 = B_M^2 - B_S^2 \quad (1)$$

The values of $B\cos\theta$ and $\sin\theta$ corresponding to each peak of the phase being investigated are plotted to make a Williamson–Hall plot. Eq. (2) is used to obtain average crystallite size and strain from the y-intercept and gradient of the linear best fit line respectively where B = broadening in FWHM due to size and strain effects (in units of radians (2θ)), θ = position of peak (in units of $^\circ\theta$), k = a constant, λ = X-ray wavelength, d = average crystallite size, η = strain [18].

$$B\cos\theta = \frac{k\lambda}{d} + \eta\sin\theta \quad (2)$$

A reference sample of high purity Al powder was used, annealed at 530 °C for 1 h in a tube with 99.998% purity argon gas pumped through at ~70 cc/min to remove any residual strains. Whilst the theoretical upper size limit of validity for this technique is around 500 nm [18], in practice it is appropriate for crystallite sizes of 10–100 nm [19]. Uncertainties became unfeasible in samples with average crystallite size over approximately 100 nm, corresponding to the samples of milling time <5 h. Therefore, values for the crystallite sizes are only given for 5–30 h. The plot of average α-Al crystallite size – calculated using the Williamson–Hall method [18] against milling time (Fig. 2a) shows a clear decreasing trend in crystallite size over 5–30 h. The plot of strain in the α-Al phase, calculated using the Williamson–Hall method, against milling time in Fig. 2b shows a clear increasing trend in strain over 5–30 h. The α-Al crystallites remain approximately constant in size after 20 h milling time. The error bars in Fig. 2 correspond to the error in the calculation of the Williamson-Hall method and the errors obtained when fitting the slope and the y-intercept values.

Based on the mastersizer results and SEM observations, the starting N powder is unimodal, with $d(0.1)$, $d(0.5)$ and $d(0.9)$ values of 16.9, 34.5 and 66.4 µm respectively. Fig. 3 plots the diameter of the 10th percentile, $d(0.1)$, the median, $d(0.5)$, and the 90th percentile, $d(0.9)$, of the powder sample particles against the logarithm of milling time. The general trends with milling time can be described as three regimes: firstly, an increase in both median size and size range up to 5 h; secondly, a significant decrease in both median size and range between 5 and 10 h; lastly, a small decrease in both median size and range after 10 h, with both parameters tending towards constant values.

Fig. 4a shows an optical image of the N alloy powder, and Fig. 4b and c shows optical images of the N8-5 and N8-30 milled nanocomposite powder respectively. It can be observed the N atomised alloy powder has a morphology consisting in rounded and elongated particles. After 5 h of milling of the nanocomposite, the N8-5 powder shows no elongated particles and with the alumina distributed in layers inside the powder particles, which was confirmed by the FIB and TEM/EDX analysis as shown in Figs. 6 and 7, respectively. Fig. 4c shows the N8-30 powder with an apparent better alumina distribution and much smaller average particle size in correspondence with the measurements obtained with the masterziser (Fig. 3).

Fig. 5 shows the DSC curves for the N powder, the N8 powders with different milling times and for the extruded sample (N8-SE). It

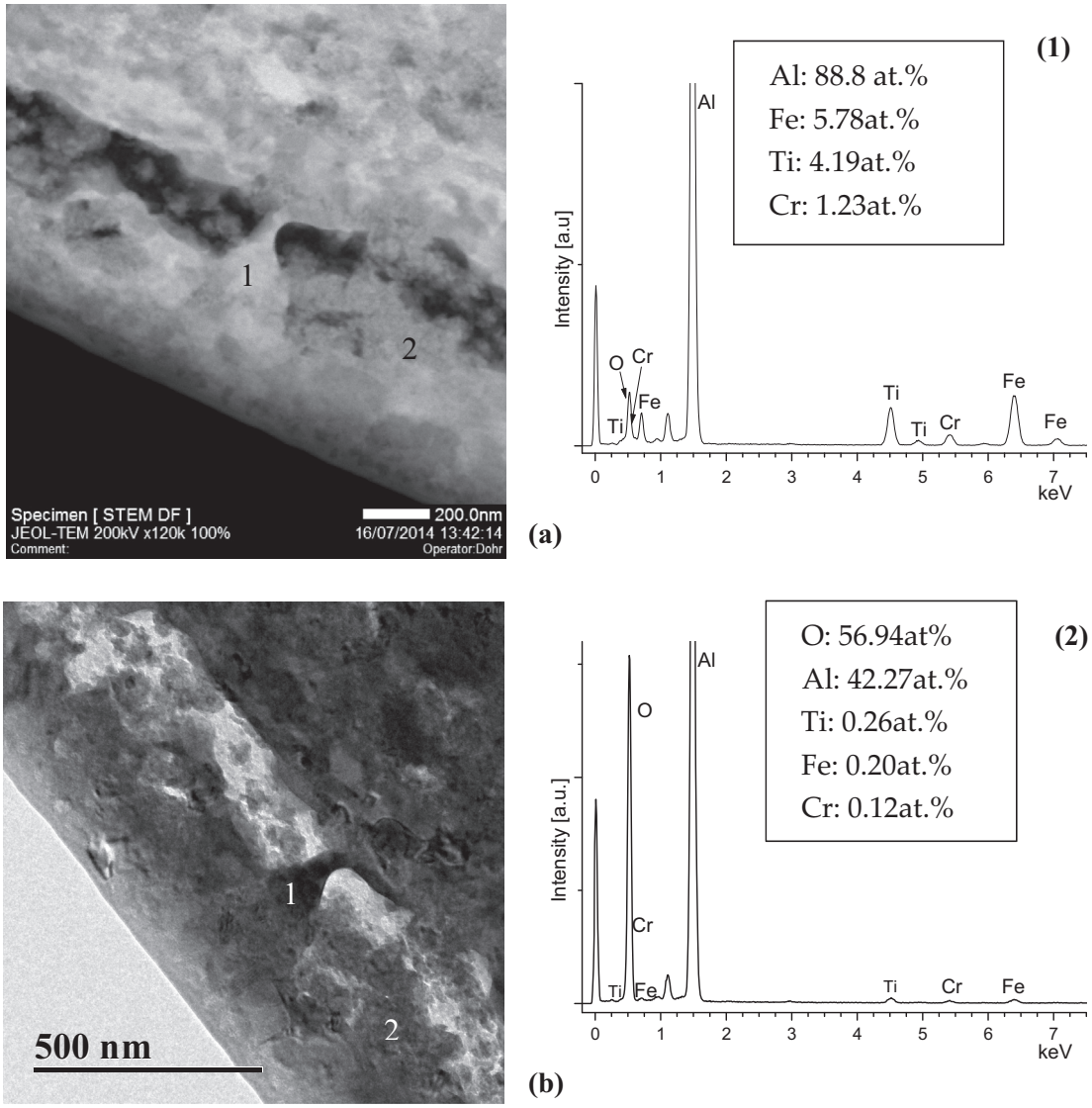

Fig. 7. N8 sample milled for 5 h. (a) STEM image showing the EDX spectra obtained for an IQC particle and Al_2O_3 regions 1 and 2 respectively. (b) Bright field TEM image.

is observed that the sample N and the N8 powders milled up to 15 h showed only one exothermic peak. The exothermic peak temperature in sample N, observed at 551.6 °C, is in agreement with the one reported in the literature for the same alloy produced by melt spinning which corresponds to the decomposition of the IQC phase [4,20–22]. The DSC curves of the powders milled from 1 to 5 h showed a linear shift of the exothermic peak towards lower temperatures, at 528.0 °C, 519.2 °C, 515.3 °C, 510.0 °C and 503.7 °C from 1 to 5 h of milling time respectively. However, this trend does not continue from 10 to 30 h of milling time; the major exothermic peak lies at 510.5 °C, 504.9 °C, 515.2 °C, 519.4 °C and 522.6 °C from 10 to 30 h of milling time respectively. Moreover, a smaller exothermic peak is observed at 435.5 °C, 441.5 °C and 444.5 °C in the DSC curves for 20, 25 and 30 h milling time respectively, showing that important changes occurred in the microstructure. Other authors, found for a melt-spun $Al_{93}Fe_3Cr_2Ti_2$ alloy an exothermic peak before the IQC phase decomposition which was assigned to intermetallic precipitation from the α-Al matrix, Audebert et al. [4] observed a peak at ~417 °C, Prima et al. [21] at ~420 °C and Galano et al. [20] at ~430 °C.

This different behaviour in the DSC curves for the two milling time ranges can be correlated with what was observed in the size distribution plot in Fig. 3. Up to 5 h of milling, the process leads to merge and weld the powders introducing a cumulative strain in the α-Al and the IQC phase increasing the free energy. This increase in the driving force for the decomposition of the IQC phase leads to a continued shifting of the exothermic peak to lower temperature. After 10 h of milling, the powder has been highly affected by the cumulative strain and high level of defects. Thus, the initial α-Al grains have developed a large quantity of subgrains reducing the average crystallite size, which appear to be stabilized after 20 h of milling (Fig. 2a). Similar trend is observed with the powder size that appears to be stabilized after 15 h of milling (Fig. 3). In this period of milling time probably a fraction of IQC phase is decomposed and dissolved in the α-Al increasing its solute content which will precipitate as intermetallics during the heating and observed in the DSC curves as a small exothermic peak before the corresponding to the IQC decomposition (see Fig. 5).

3.1.2. Distribution of reinforcement

Fig. 6 shows FIB images of the powders milled for different lengths of time. Heterogeneity of the reinforcement distribution is manifested as regions of matrix containing no reinforcement, and agglomerations of reinforcement, for milling times below

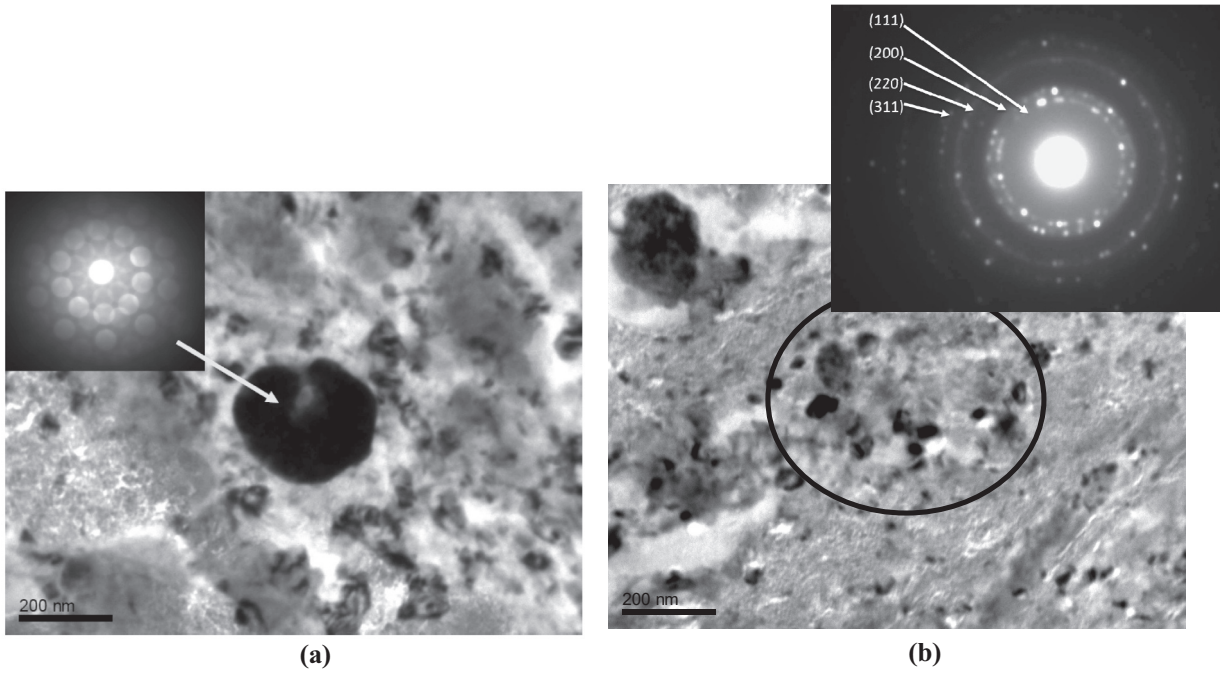

Fig. 8. Bright field TEM images of the N8 powder sample milled for 10 h. (a) A quasicrystalline particle (as confirmed by the 5-fold CBDP) embedded in the matrix. (b) α-Al crystallites in the matrix (as confirmed by the SAD pattern).

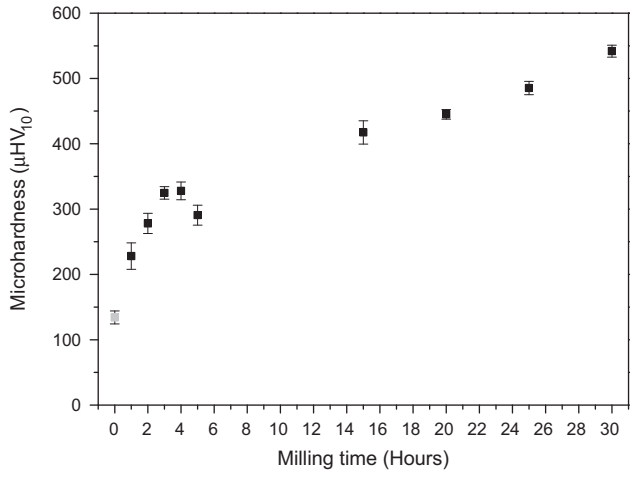

Fig. 9. Microhardness of N8 powder specimens plotted against milling time up to 30 h. The data point for 0 h corresponds to the N powder.

15 h. It can be seen that at 1 h of milling time, there is very little reinforcement present within the powder particles, and is mostly still coated to the outside of the matrix particles. Heterogeneity is in the order of 10 s of microns. Between 1 h and 10 h there is a noticeable improvement in the distribution: significant quantities of reinforcement are present within the particles, although there is still heterogeneity on the order of microns at 10 h. The improvement in the uniformity of distribution between 10 h and 15 h is very fast in comparison to the more incremental rate of change of distribution uniformity observed over other 5 h periods, as the scale of heterogeneity is reduced to 100 s of nm. From 20 h onwards, improvement is incremental. After 30 h, there are still few agglomerates of reinforcement and unreinforced regions of matrix.

Between 5 and 10 h, the mean particle size decreases from 96 μm to 17 μm (Fig. 3). This decrease in particle size would result in large areas of 'fresh' particle surface to be exposed, and thus to be coated in reinforcement, over a short time period. It would then take further time for this reinforcement to be distributed within the powder, by cold-welding and fracture. Fracture by interfacial decohesion and void coalescence is a function of the spacing of particles and particle size. It can therefore be predicted that since the average size, size range and concentration of agglomerates is seen to decrease with milling time, the fracture toughness will increase with milling time.

Powders were characterised by TEM. Fig. 7 shows a representative TEM image from the powders milled for 5 h (N8-5) with its corresponding STEM image. EDX spectrum and compositions are shown for two representative phases: a quasicrystalline particle (1) which compositions related to the one reported in literature [5,6] and (2) an area in the matrix showing the presence of Al_2O_3.

Fig. 8 shows representative TEM images for powders milled for 10 h (N8-10). Fig. 8a shows the presence of an IQC particle as verified by the convergent beam diffraction pattern (CBDP) and Fig. 8b shows a general area of the powder particle showing the Al crystallites. The crystallite sizes were measured by drawing a vertical and a horizontal line on each crystallite. The length of the two perpendicular lines crossings each crystallite size was measured and the average value was taken as the size of the particle. About 50 crystallites of each sample were measured to ensure an accurate value. This process was repeated for powders with different milling times. Thus, it was obtained that the crystallite sizes for N8-10 is 81 ± 18 nm and 53 ± 9 nm for N8-15. Both these values are in agreement with the values obtained by the XRD results (Williamson–Hall method) which gave 89 nm and 51 nm respectively (see Fig. 2a).

The microhardness of the powders is shown in Fig. 9. The hardening curve has two distinctive regimes. A steep hardening gradient between 0 and 4 h of milling, and a shallower, linear gradient from 15 h onwards. No 10 h data point is given as the indentations for this powder were not regular enough to be measured. Again, the microhardness evolution with the milling time shows two different regimens, one up to ~5 h and other after 15 h; similar as was

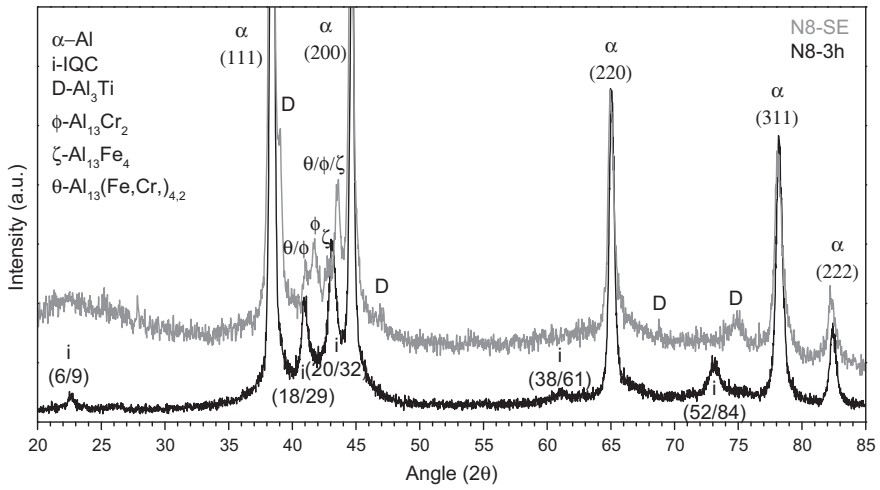

Fig. 10. X-ray diffractograms of the N8-3h milled powder, and the powder from the N8-SE extruded composite.

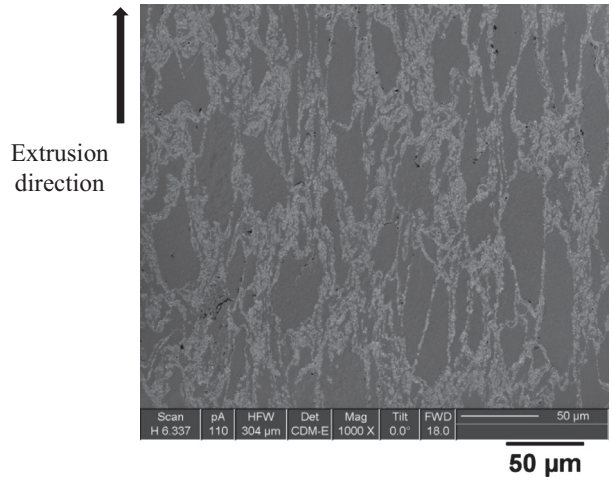

Fig. 11. FIB image of the longitudinal section of N8-SE. The Al_2O_3 net microstructure can be observed.

observed for the α-Al crystallite size distribution plot (Fig. 3), in the DSC curves (Fig. 5) and the reinforcement distribution observed in FIB (Fig. 6). This suggests that an intermediate regime exist between ~5 h and ~15 h.

3.2. Extruded samples

From theory, it is expected that crystallite size and strain decrease and increase respectively with the logarithm of milling time [19]. Since the uniformity of reinforcement is partially dependent on the cumulative strain, it is therefore expected that the average spacing between reinforcement particles decreases approximately with the logarithm of milling time too. Thus, the composite will highly increase the strength by Hall–Petch and Orowan mechanisms for a homogeneous particle distribution, which it is expected to be obtained for an extruded bar of powder milled for around 30 h. This long processing time implies an expensive manufacturing process therefore it is worth studying the microstructure and properties of a composite extruded from powders that does not have a complete homogenous reinforcement distribution.

The X-ray diffractogram for the N8-SE extruded bar in comparison to the N8-3 ball milled powder are shown in Fig. 10. The phases α-Al, Al_3Ti, $Al_{13}Cr_2$, $Al_{13}Fe_4$ and the metastable distorted θ-$Al_{13}(Fe,Cr)_{2-4}$ have been identified in the extruded sample [4,5,17]. No IQC phase peaks were identified in the extruded bar, however it is observed in the N8-3 powder sample. In addition, the IQC decomposition peak is present in the DSC curve for the ball milled powder N8-3, but not in the DSC curve of the N8-SE extruded sample. These three observations show that the IQC phase has decomposed into intermetallics during extrusion.

The FIB image in Fig. 11 shows the heterogeneity that exists at different length scales in the longitudinal sections of N8-SE. As the N8-3 powder does not have a homogeneous distribution, the extruded sample showed an Al_2O_3 net microstructure slightly deformed in the extrusion direction.

The μHV_{500} values for the extruded specimens were 159 ± 1 for the N-SE (sample of the N alloy extruded under the same conditions as N8-SE) and 227 ± 3 for the composite N8-SE. Thus, even though the extruded composite has an Al_2O_3 net microstructure instead of a homogeneous distribution of the Al_2O_3 reinforcement in the nanoquasicrystalline alloy matrix, the addition of 8.5 vol.%Al_2O_3 and the ball milling process for only 3 h have increased the hardness by ~43% respect to the extruded alloy. Therefore, it seems that the decomposition of the IQC phase during the hot extrusion did not have an important detrimental effect on the improvement in the strength of the composite.

4. Conclusions

A new metal matrix composite has been produced having a nanoquasicrystalline $Al_{93}Fe_3Cr_2Ti_2$ alloy matrix reinforced by 20–50 nm γ-Al_2O_3 particles, partially distributed by means of ball milling. To the best of the authors' knowledge it is the first time that this new nanoquasicrystalline alloy matrix composite has been studied.

The ball milling process to produce that composite powder shows three different steps as function of the milling time. A first step can be defined up to around 5 h of milling, where the rate of microstructural change is fast as well as the work hardening. Metastable phase (distorted θ-phase) precipitates and then dissolves in the matrix, the IQC phase increases its free energy decreasing its decomposition temperature and the powder particle size increases remarkably with a sluggish reinforcement distribution.

A second step can take place between 5 h and 15 h of milling, where the cumulative strain leads to a strong decrease of the α-Al crystallites size without noticeable phase transformations. The powder particle size decreases abruptly, the homogeneity of the

reinforcement distribution increases faster and the work hardening rate reduces in comparison with the first regime.

The third step that can be defined from ~15 h of milling onwards, is more stable than both of the previous steps. The α-Al crystallite size slightly decreases and remains practically constant with the milling time after 20 h of milling; the powder particle size shows similar behaviour. The IQC phase begins to decompose slowly with the milling time and the γ-Al_2O_3 is becoming more homogenously distributed reducing the average distance between the reinforcement particles. As the α-Al crystallite size remains constant only the γ-Al_2O_3 distribution continues contributing to strengthen the composite, thus it is observed that the work hardening increases with a lower and constant rate.

An extruded bar from an inhomogeneous distribution of the γ-Al_2O_3 particles in the nanoquasicrystalline matrix, shows an Al_2O_3 net microstructure with ~43% higher hardness than the un-reinforced extruded $Al_{93}Fe_3Cr_2Ti_2$ alloy. The IQC phase is decomposed during the extrusion process at a temperature of 475 °C ± 20 °C.

It is expected that manufacturing of this new composite by extrusion at lower temperature will allow retaining the icosahedral quasicrystalline phase and thus the mechanical properties will be enhanced even further.

Acknowledgements

The authors thank Alpoco Ltd. company for their support of the project. The authors also appreciate the support of Dr. G. Chapman and Dr. N. Young for assisting with the SEM and TEM/STEM techniques and Dr. Kerstin Jurkschat for assistance with the Mastersizer. Prof. M. Galano thanks the RAEng for the support in research through a Research Fellowship EP/G05794X/1. This work was partially supported by the cooperation project PICT-Oxford 2831 and UBACYT 2010/058 grants. Prof. F. Audebert thanks CONICET.

References

[1] A. Knowles, X. Jiang, M. Galano, F. Audebert, Microstructure and mechanical properties of 6061 Al alloy based composites with SiC nanoparticles, J. Alloys Comp. 615 (2014) s401–s405.
[2] A. Inoue, Amorphous, nanoquasicrystalline and nanocrystalline alloys in Al-based systems, Prog. Mater. Sci. 43 (1998) 365–520.
[3] M. Galano, F. Audebert, A. García-Escorial, I.C. Stone, B. Cantor, Nanoquasicrystalline Al–Fe–Cr-based alloys. Part II: mechanical properties, Acta Mater. 57 (2009) 5120–5130.
[4] F. Audebert, F. Prima, M. Galano, M. Tomut, P.J. Warren, I.C. Stone, B. Cantor, Structural characterisation and mechanical properties of nanocomposite Al-based alloys, Mater. Trans. 43 (2002) 2017–2025.
[5] M. Galano, F. Audebert, I.C. Stone, B. Cantor, Nanoquasicrystalline Al–Fe–Cr-based alloys. Part I: phase transformations, Acta Mater. 57 (2009) 5107–5119.
[6] N. Rounthwaite, Development of bulk nanoquasicrystalline alloys for high strength elevated temperature application, DPhil Thesis, the University of Oxford, 2012.
[7] I. Todd, Z. Chlup, J. O'Dwyer, M. Lieblich, A. García-Escorial, The influence of processing variables on the structure and mechanical properties of nano-quasicrystalline reinforced aluminium alloys, Mater. Sci. Eng. A 375 (2004) 1235–1238.
[8] Y.C. Kang, S.L.I. Chan, Tensile properties of nanometric Al_2O_3 particulate-reinforced aluminum matrix composites, Mater. Chem. Phys. 85 (2004) 438–443.
[9] M. Tavoosi, F. Karimzadeh, M. Enayati, Bulk Al–Zn/Al_2O_3 nanocomposite prepared by reactive milling and hot pressing methods, Mater. Lett. 62 (2008) 282–285.
[10] H. Ahamed, V. Senthilkumar, Experimental investigation on newly developed ultrafine-grained aluminium based nano-composites with improved mechanical properties, Mater. Des. 37 (2012) 182–192.
[11] B. Prabhu, C. Suryanarayana, L. An, R. Vaidyanathan, Synthesis and characterization of high volume fraction Al–Al_2O_3 nanocomposite powders by high-energy milling, Mater. Sci. Eng. A 425 (2006) 192–200.
[12] Z.R. Hesabi, A. Simchi, S. Reihani, Structural evolution during mechanical milling of nanometric and micrometric Al_2O_3 reinforced Al matrix composites, Mater. Sci. Eng. A 428 (2006) 159–168.
[13] Y. Mazaheri, F. Karimzadeh, M.-H. Enayati, Nanoindentation study of Al356–Al_2O_3 nanocomposite prepared by ball milling, Mater. Sci. Appl. 1 (2010) 217.
[14] J.W. Cahn, D. Shechtman, D. Gratias, Indexing of icosahedral quasiperiodic crystals, J. Mater. Res. 1 (1986) 13–26.
[15] K. Shirasuka, H. Yanagida, G. Yamaguchi, The preparation of η-alumina and its structure, J. Ceram. Assoc. Jpn. 84 (1976) 610.
[16] Y. Rozita, R. Brydson, A. Scott, An investigation on commercial gamma Al_2O_3 nanoparticles, J. Phys. Conf. Ser. 241, IOP Publ. (2010) 012096.
[17] R. Manaila, V. Florescu, A. Jianu, O. Radulescu, On the transition-metal quasisublattice in icosahedral Al–Cr–Fe phases, Philos. Mag. B 60 (1989) 589.
[18] C. Suryanarayana, M.G. Norton, X-ray Diffraction: A Practical Approach, Plenunm Press, New York, 1998.
[19] C. Suryanarayana, Mechanical alloying and milling, Prog. Mater. Sci. 46 (2001) 1–184.
[20] M. Galano, F. Audebert, B. Cantor, I.C. Stone, Structural characterisation and stability of new nanoquasicrystalline Al-based alloys, Mater. Sci. Eng. A 375–377 (2004) 1206–1211.
[21] F. Prima, M. Tomut, I.C. Stone, B. Cantor, D. Janickovic, G. Vlasak, P. Svec, In situ resistometric investigation of phase transformations in rapidly solidified Al-based alloys containing dispersed nanoscale particles, Mater. Sci. Eng. A 375 (2004) 772–775.
[22] M. Galano, F. Audebert, A. García-Escorial, I.C. Stone, B. Cantor, Nanoquasicrystalline Al–Fe–Cr-based alloys with high strength at elevated temperature, J. Alloys Comp. 495 (2010) 372–376.